Evaluating carbon extremes in a coupled climate-carbon cycle simulation

1st Min Xu
Computational Sciences and Engineering Division
Oak Ridge National Laboratory
Oak Ridge, USA
xum1@ornl.gov

2nd Salil Mahajan
Computational Sciences and Engineering Division
Oak Ridge National Laboratory
Oak Ridge, USA
mahajans@ornl.gov

3rd Forrest M. Hoffman
Computational Sciences and Engineering Division
Oak Ridge National Laboratory
Oak Ridge, USA
forrest@climatemodeling.org

4th Xiaoying Shi
Climate Change Science Institute
Oak Ridge National Laboratory
Oak Ridge, USA
shix@ornl.gov

***Abstract*—Gross primary production (GPP) measures the photosynthetic update of carbon by terrestrial ecosystems. Accurately quantifying and simulating GPP and its extremes remains a challenge in global carbon cycle sciences. Here, we evaluate GPP extremes in a coupled biogeochemistry (BGC) simulation by the Department of Energy's Energy Exascale Earth System Model (E3SMv1.1) using the Generalized Extreme Value (GEV) distribution statistical model. The simulation is evaluated against the Global Bio-Atmosphere Flux (GBAF) data. Temporal trends and ENSO dependence are also investigated by using GEV models where time and the Niño3.4 index are introduced as linear covariates. The E3SMv1.1 model simulation generally predicts stronger negative and positive GPP extremes as compared to GBAF data. It also tends to simulate stronger temporal trends of GPP extremes than GBAF data. While negative GPP extreme trends are not significant in either E3SM or GBAF, positive GPP trends are statistically significant over several regions only for the E3SMv1.1 model simulation. ENSO dependence is generally stronger in the E3SMv1.1 model simulation, but ENSO dependence is found not to be significant for the time period analyzed (1980-2006) to match GBAF data. For the longer simulation period of 1900-2006, ENSO dependence is found to be statistically significant over Amazon, the maritime continent and Northern Australia for both negative and positive extremes.**

***Index Terms*—carbon extremes, GEV statistical model, terrestrial ecosystem, carbon cycle**

I. Introduction

Continuous increases in the concentrations of radiatively active greenhouse gases in the atmosphere, especially carbon dioxide (CO_2) caused by human activities, are greatly altering the Earth's climate [1] and significantly enhancing climate extremes [2], [3], [4]. Furthermore, Baker et al. [5] suggested that rising atmospheric CO_2 concentration ($[CO_2]$) may lead to an increase in extreme weather and climate events even if the increase in average global temperature remains at a certain level.

The terrestrial ecosystem plays an important role in global carbon cycle and dynamics as it is the third largest carbon pool right after the ocean and geological pools [6]. Moreover, it generally uptakes atmospheric CO_2 through vegetation photosynthesis. This part of carbon is then cycled through ecosystems and can be released back to the atmosphere by autotrophic (plant) and heterotrophic (soil microbial and animal) respiration and additional disturbances [7]. However these processes are complex and highly uncertain [6] and could lead to large biases in projections of future CO_2 concentration [8].

The terrestrial ecosystem usually is a net carbon sink. Studies show that approximately 25–30% of anthropogenic CO_2 emission have been uptaken by it for the past 50 years since 1958 [6] [9]. Gross primary production (GPP) measures the photosynthetic uptake of CO_2 by the terrestrial ecosystem and is strongly controlled by climate including temperature, precipitation, and radiation. Moreover climate extremes including drought, flood, heat wave and cold spell have significant impacts on the carbon uptake capability of the terrestrial ecosystem. For example, The 2010 Amazon drought [10] killed tremendous trees and greatly reduced carbon uptake by the vegetation. It caused the release of nearly 500 million tons of carbon (1.8 billion tons of carbon dioxide) into the atmosphere in Amazon during the event [11].

Therefore, better understanding the characteristics and trends of carbon (like GPP) extremes is of great importance for us to study complex biogeochemical feedbacks to climate for accurately predicting the effects and extent of climate change [1]. It could also improve representations of the interactions between climate and the carbon cycle in Earth System Models (ESMs) [3].

Here, we evaluate carbon extremes in a coupled climate-carbon simulation by the Department of Energy (DOE)-Energy Exascale Earth System Model (E3SM). We apply the Generalized Extreme Value (GEV) statistical model on

2375-9259/19/$31.00 ©2019 IEEE
DOI 10.1109/ICDMW.2019.00052

the monthly GPP outputs from the simulation. Generalized Extreme Value (GEV) distribution is a family of continuous and asymptotic limit probability distributions for maxima or minima derived from a sequence of random variables with a predefined fixed block size. It has been widely used in studying climate extremes, e.g. precipitation, temperature, wind etc. [12]–[18]. But, there are only a few studies that use the GEV modeling approach on carbon extremes. For example, Sippel et al. [19], [20] applied the GEV model to examine the discrepancies of GPP extremes in the bias-corrected ensemble simulations and observations. Some studies [21], [22] used GEV to fit the normalized difference vegetation index (NDVI) data from satellite remote sensing. NDVI generally is a good proxy of GPP and highly correlated with it. Previous studies of carbon extremes largely use percentile-based definitions of extremes [23], [3], [24]. GEV models of extremes provide a more comprehensive examination of extremes allowing for extrapolation of extremes and computation of return period of extreme events of different magnitudes.

We focus our study on (1) characterizing the stationary and non-stationary statistics of GPP extremes using GEV; and (2) quantifying the dependence of GPP extremes on an important large scale climate variability (i.e. El Niño-Southern Oscillation (ENSO)).

II. Model Experiments, Data and Methodology

A. E3SM model

The DOE E3SM model is an earth system model that can simulate states of the coupled climate containing the atmosphere, ocean, cryosphere, land surface, and biogeochemistry (BGC). Its version 1.0 was used to simulate the full suite of Diagnosis, Evaluation, and Characterization of Klima (DECK) experiments of the sixth phase of coupled model intercomparison project (CMIP6) [25], which was described by [26]. Burrows et al. [27] introduced the E3SMv1.1-BGC and described the coupled biogeochemical simulations using it. Compared to the E3SMv1, the E3SMv1.1-BGC includes some important bug fixes and major features of the carbon cycle and biogeochemical processes including a land model with prognostic carbon, nitrogen, and phosphorus in multiple pools and nutrient regulations on photosynthesis. Beside the above, it also includes an active, coupled ocean and sea ice biogeochemistry model based on the Biogeochemical Elemental Cycling (BEC) model [28], [29]

Here, we analyze the monthly GPP outputs for the period of 1900-2006 from the historical simulation by the coupled E3SMv1.1-BGC model. The simulation accounted for the effects of the atmospheric CO_2 both on the radiative and biogeochemical processes and defined the atmospheric CO_2 concentration by its contemporary trajectory [8]. Other forcings including nitrogen deposition, land use and land cover changes and aerosols are included in the simulation too. The coupled BGC simulation by the E3SMv1.1-BGC is hereafter referred to as the E3SM-BGC.

B. Data

The Global Bio-Atmosphere Flux (GBAF) data, also known as FLUXET-MTE, are global estimates of carbon and water fluxes that empirically upscale FLUXNET eddy covariance measurements using the multi-tree model (MTE) method and the LundPotsdamJena Managed Land (LPJmL) model outputs [30], [31]. We used the GBAF monthly GPP product in a spatial resolution of 0.5 by 0.5 degree from 1982 to 2008 to evaluate GPP extremes in the E3SM-BGC simulation.

C. GEV

We apply the generalized extreme value (GEV) distribution statistical models to quantify GPP extremes and their non-stationarity. To identify temporal trends in GPP extremes we use time as a covariate in a GEV model. Additionally, we quantify the impact of ENSO on carbon extremes by using the Niño3.4 index in another GEV model. Here, we use the block maximum/minimum approach to model extremes using GEV. We fit GEV distributions to either annual (block size of one year) maximum (or minimum) GPP anomalies of monthly averages at each grid point using the R package *ismev* [32]. Here, the anomalies at each grid point refer to the remainder after removing the annual cycle in monthly average GPP there. Similar covariate-based block maxima/minima and peak over threshold approaches using GEV are now commonly applied to evaluate climate extremes and their non-stationarity [13]–[15], [17].

Extreme value theory postulates that the block (defined as non-overlapping segments of equal size of the data record, for e.g. 1yr, 5yr, etc.) maximum or block minimum of independently and identically distributed samples follow a family of three parameter GEV distribution, GEV(μ, σ, ξ), which is represented as:

$$G(z) = \exp\left\{-[1 + \xi(\frac{z-\mu}{\sigma})]^{-1/\xi}\right\} \quad (1)$$

where μ, σ and ξ represent the location, scale and shape parameter respectively of the distribution. For $\xi = 0$, the function is computed as the limit of the equation as $\xi \to 0$ [33]. Return periods of extremes can be easily from the GEV parameters by inverting the equation [33]. Here, we compute the parameters of the GEV(μ, σ, ξ) model by the maximum log-likelihood method, which maximizes the probability of the occurrence of each of the used block maximum (or minimum) values in $G(z)$. The sampling frequency of data for estimating the GEV is chosen based on the availability of data used. For the GBAF data, monthly averages of GPP for the period of 1982-2008 were available. So, we used annual maxima/minima of monthly anomalies for estimating GEVs. We also quantify extremes in the E3SM simulations in a similar way for the period of 1980-2006 to evaluate the simulations against the GBAF data.

A GEV model is fit to data at each grid point. The base GEV model with no covariates is termed as the BaseGEV model, and is referred as such hereafter. A Kolmogrov-Smirnov (KS) goodness of fit test is conducted at each grid point to evaluate

if a significant discrepancy exists between the fitted data and the GEV model representing the data. Significant auto-correlation may be present in annual maxima/minima of GPP data which would imply that the data is not independent as assumed for the GEV fit, which may result in a poor fit [18]. We do not evaluate the impact of auto-correlation on GEV fits to GPP data here, which will be a subject of future study. But, previous studies indicate that presence of auto-correlation does not invalidate the use of GEV to study block extremes of climate variables like temperature and precipitation, and it also does not always lead to a poor GEV fit [17], [18].

Non-stationary in GPP extremes here is captured by a linear time-dependent (or dependent on some other index) parameter in μ:

$$\mu = \mu_0 + \alpha_t \cdot t \tag{2}$$

We thus modify the BaseGEV model to include a time index as a covariate in the location parameter term, where t is the year (ranging from 1982 to 2008 for the GBAF data, for example), and α_t represents the linear rate of change of the location parameter with time. This additional GEV model parameter in $GEV(\mu_0 + \alpha_t \cdot t, \sigma, \xi)$, is also computed by the maximum log-likelihood method along with the other model parameters. We call this new GEV model the timeGEV model, hereafter. Non-linear trends as well as trends in the σ and ξ will be a subject of future studies and are not investigated here. Previous studies have found significant temporal trends in σ for climate variables like temperature and precipitation [18].

Likewise, we modify the BaseGEV model to include the Niño3.4 index as a linear covarite in the location parameter to quantify the impact of ENSO on GPP extremes, $\mu = \mu_0 + \alpha_{ENSO} \cdot Ni\tilde{n}o3.4(t)$, where α_{ENSO} represents the linear rate of change of the location parameter with the Niño3.4 index, and $Ni\tilde{n}o3.4(t)$ represents the annual average Niño3.4 index at year, t. We refer to this GEV model as the ENSOGEV.

We use the likelihood-ratio test to establish if the timeGEV and the ENSOGEV models are significantly different from the BaseGEV model - that is, if the new co-variate terms α_t and α_{ENSO} are statistically different from zero. The deviance statistic for the likelihood test is defined as the difference in the maximized log-likelihoods between a new GEV model and the base GEV model [33], and is computed at each grid point. The null hypothesis that the new GEV model and the base GEV model are statistically equivalent is rejected if the p-value of the deviance statistic is less than a a given critical value (c).

Since we conduct the likelihood ratio test at each grid point, we are conducting multiple hypothesis tests (N tests, one for each grid point) simultaneously. The critical value of a test, c, is generally the given significance level of testing (β, say 0.05), but only when we test a single hypothesis test. The significance level that governs the $\beta \cdot N$ tests would yield false rejections of the null hypothesis, just by chance, if N hypothesis tests were conducted [34]. Thus, the critical value needs to be adjusted to account for multiple hypothesis tests and control for erroneously rejecting true null hypotheses. This is achieved here by using the false discovery rate (FDR) approach [34], [35] similar to some previous studies [17], [18]. The FDR approach states that for a given significance level (β), the critical value should be adjusted when conducting multiple hypothesis tests simultaneously as follows:

$$c_{FDR} = \max_{i=1,2,\ldots,N} \{p_i : p_i \leq \beta(\frac{j}{N})\} \tag{3}$$

where, p_j represents the p-value of the deviance statistic for grid-point i, and N is the total number of grid points.

Thus, a null hypothesis for a grid point under the FDR approach at a significance level of β is now rejected only if the p-value of the deviance statistic is less than c_{FDR} instead of β. Also, it should be noted that using the FDR approach also automatically tests for field significance [34]. That is, even a single grid point rejecting the null hypothesis using c_{FDR} implies that the global null hypothesis - that the local null hypothesis is true for all grid points - is rejected too [34], [35].

III. Results and Discussions

A. *GPP Extremes*

Fig. 1 a and b show the geographic distribution of the GEV location parameters (μ) for the BaseGEV model derived from the annual block minima of monthly GPP anomalies for the E3SM-BGC simulation for the period of 1980-2006 and the GBAF observation for the period of 1982-2008 respectively. White areas over land denotes grid points where the GEV fit did not converge or where the KS goodness of fit test indicated a poor GEV model fit. Negative values of GPP anomalies indicate GPP reduction and imply carbon loss to the atmosphere, thus, the annual block minima of negative anomalies represents negative GPP extremes. Larger magnitude of negative values of μ thus indicate stronger extreme GPP loss.

The model simulated negative GPP extremes are generally very severe in the tropical and subtropical areas where the GBAF data show strongest GPP loss extremes too, including northeastern and eastern Amazon, U.S. Midwest, central America, western central Africa, southern Africa, India, southern Asia, northern China and eastern coast of Australia. While in Canada, Eurasia and Northern Africa the model simulation negative GPP extremes are weaker (magnitudes less than 0.8 gCm^2day^1) due to the lower average GPP. Though the overall spatial pattern is similar between the model simulated and GBAF μ, model simulated μ is much larger than that of GBAF, nearly globally, by as large as a factor of three or larger in some regions (Fig. 1b). The model performs better at regions with weak negative GPP extremes with similar magnitudes as the GBAF data, for example, over central and Northern Asia and western coast of South America.

Zscheischler et al. [23] identified spatiotemporal contiguous extreme anomalies in four global monthly GPP data sets including FLUXNET-MTE (GBAF), MOD17+, LPJmL and OCN from 1982 to 2011. The GPP extremes are defined by

a certain percentile (larger than the 90^{th}) on the absolute values of the anomalies and then are merged into an extreme events using a contiguous algorithm. Our results are in good agreement with theirs as regards the global pattern of the hot spot of negative GPP extremes. The magnitudes of negative GPP extremes in the FLUXNET-MET(GBAF) are 3 to 4 times less than those in the model simulations of LPJmL and OCN and a little bit less than those in the MODIS GPP data. The strong negative GPP extremes in northeastern Amazon in the E3SM-BGC simulation are also observed in the MODIS GPP data. Moreover Zscheischler et al. [3] applied the same method of [23] to the GPP and net ecosystem production (NEP) outputs of the CMIP5 multi-model ensemble. The spatial pattern of negative GPP extremes in the E3SM-BGC simulation agrees very well with that of CMIP5 multi-model ensemble.

Chen et al. [24] defined extremes as the negative 5^{th} percentile of GPP anomalies and further combined the extremes into individual extreme events using a three-dimensional contiguous algorithm. Then they applied the method on monthly GPP outputs from 1982-2015 simulated by 12 process-based models in the TRENDY project to study the spatiotemporal patterns of negative GPP extremes in China. Their results showed that in the TRENDY models, hotspots of negative GPP extremes majorly happened in northern China which is consistent with our results. They attributed the negative GPP extremes to frequent drought occurring in northern China.

The spatial pattern of location parameters of positive GPP extremes is very similar to that of negative extremes, both from the GBAF data as well as E3SM-BGC simulation (Fig. 2 a,b), with stronger extremes occurring over eastern Amazon, U.S. Midwest, central America, western central Africa, India, southern Asia and eastern coast of Australia. Again, similar to negative GPP extremes, model simulated positive GPP extremes are much stronger that those of the GBAF data over regions with strong extremes by about a factor of three or larger. While over regions with weak extremes the E3SM simulation matches well with the GBAF data, for example over North America, central Asia, northern Europe and eastern coast of South America.

Compared with negative GPP extremes, the magnitudes of μ of positive GPP extremes are generally 50-70% less than those of negative GPP extremes both for the E3SM-BGC simulation and GBAF data. The asymmetry between positive and negative GPP extremes were also seen in the FLUXNET-MTE, MOD17+, LPJmL and OCN data sets [23] and the CMIP5 model ensemble [3].

B. Non-stationarity of GPP extremes: Trends

Fig. 3 shows the coefficient α_t representing the linear temporal trend in the location parameters as estimated for the timeGEV model of negative GPP anomalies for the E3SM-BGC simulation (over the period of 1982-2008) and GBAF data (1980-2006). Positive trends indicate a decrease in the intensity of negative GPP extremes. Trends in the E3SM-BGC simulation are generally stronger than the GBAF data.

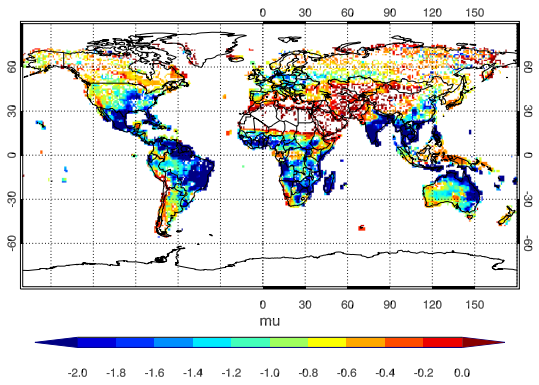

(a) E3SM-BGC: Negative GPP Extremes

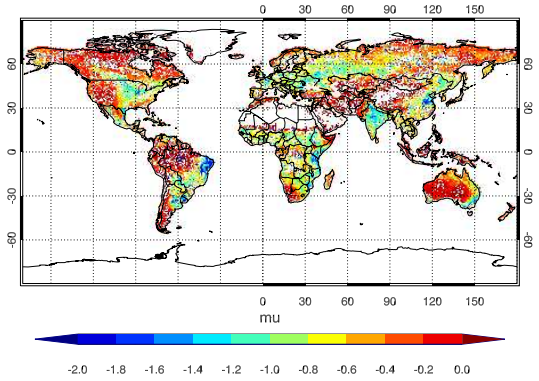

(b) GBAF: Negative GPP Extremes

Fig. 1: Geographic distribution of the location parameter of GEV fits to annual block minima of monthly GPP anomalies (units: $gCm^{-2}day^{-1}$) of (a) the E3SM-BGC simulation (1980-2006) and (b) the observational data product GBAF during 1982-2008). White areas over land denotes grid points where a KS goodness of fit test indicates a poor GEV model fit.

However, it should be noted that almost no land grid points show statistical significance at the 95% confidence level based on the FDR approach of multiple hypothesis tests for both the model simulation and GBAF data.

Fig. 4 shows the trend, α_t, in μ for positive GPP extremes. There are statistically significant (at the 95% confidence level) large positive trends over the Amazon, western Africa, Eurasia, southeastern China, southeastern Australia and the maritime continent in the E3SM-BGC simulation (Fig.4). The strongest trends in the GBAF data are observed over western Africa, southern European, India and Southeastern China, similar to the E3SM simulation, but these observed trends are much weaker and not statistically significant.

In regions of Amazon, western Africa, Eurasia, and Indonesia there are strong positive trends both for negative and positive GPP extremes and the trends for positive GPP extremes are generally larger than those for negative extremes. It indicates that in these regions CO_2 fertilization plays a important role in the increases in positive GPP extremes. In

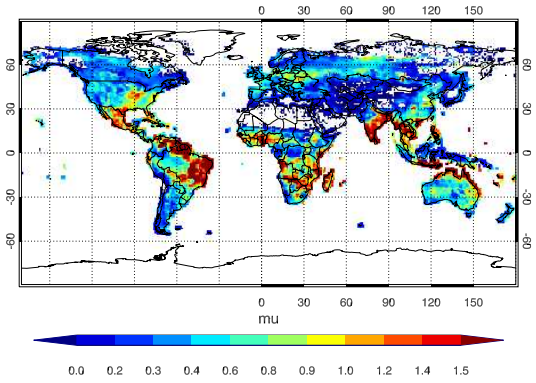

(a) E3SM-BGC: Positive GPP Extremes

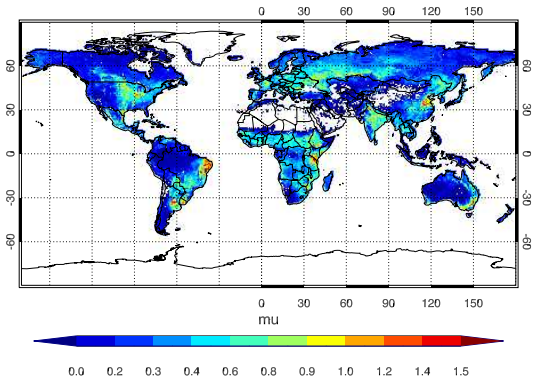

(b) GBAF: Positive GPP Extremes

Fig. 2: Same as Fig. 1, except for annual block maxima.

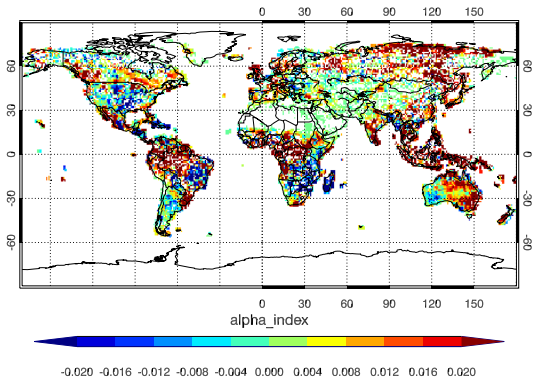

(a) E3SM-BGC: Trend in Negative GPP Extremes

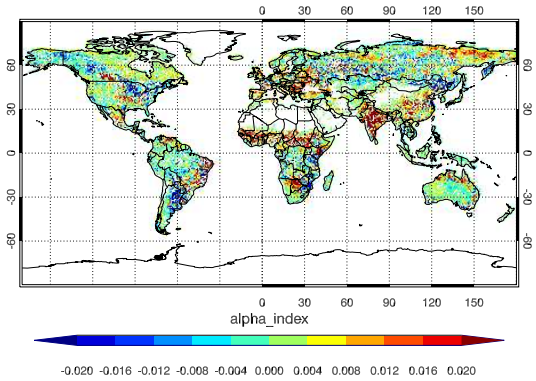

(b) GBAF: Trend in Negative GPP Extremes

Fig. 3: Geographic distribution of the linear trend, α_t, in the GEV location parameter for timeGEV model of annual block minima (units: $gCm^{-2}day^{-1}year^{-1}$) of (a) the E3SM-BGC simulation (1980-2006) and (b) the GBAF data during 1982-2008. Hatching represents regions where timeGEV is statistically different than BaseGEV at the 95% confidence level (based on the log-likelihood test and using the false discovery rate approach for establishing statistical significance. Please see main text's Section IIc.)

southern Africa, western and central U.S. there are strong negative trends for negative GPP extremes while weak positive trends for positive GPP extremes. However there are no apparent differences in the trends between negative and positive GPP extremes in the GBAF data.

There are some studies on the trend of GPP extremes, e.g. [3], in which they analyzed the trends of global averaged negative and positive GPP extremes. But here we evaluate the trends of negative and positive GPP extremes in each grid cell and examine their global geographical distribution patterns.

C. *ENSO impact on GPP extremes*

Fig. 5 and Fig. 6 show the ENSO-dependent component α_{ENSO} of μ of the respective ENSOGEV models for annual maxima and minima. For negative GPP extremes, ENSO dependence in the E3SM-BGC simulation is generally larger than the GBAF data. However, this ENSO dependence is found not to be statistically significant almost everywhere. Interestingly, ENSO dependence is found to be of opposite sign in the Amazon region, central U.S., southern Asia (Fig. 5) between the model simulation and GBAF data. While the model results indicate that stronger ENSO events lead to more severe negative GPP extremes in these regions, the GBAF results show the opposite effect.

Since the GBAF GPP dataset is a upscaling product in which it is hard to account for effects of disturbance and/or site history and lagged environmental effects [30], it may cause the discrepancy in the ENSO dependence for the negative GPP extremes between the E3SM-BGC and GBAF data. In the future, we will use the MODIS and other GPP products and long-term site observations to study the uncertainty in the observations.

For the positive GPP extremes (Fig. 6), again, ENSO dependence is found not be statistically significant almost everywhere for both the E3SM-BGC simulation and GBAD data. Nonetheless, we note that there are large negative trends in northeastern and eastern Amazon, India, southeast Asia, northern Australia and southern maritime continent; and large positive trends in central U.S. and southeastern South America. Compared with the model results, the magnitudes of the trends

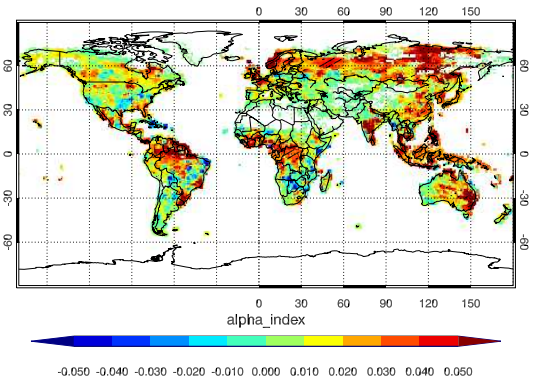

(a) E3SM-BGC: Trend in Positive GPP Extremes

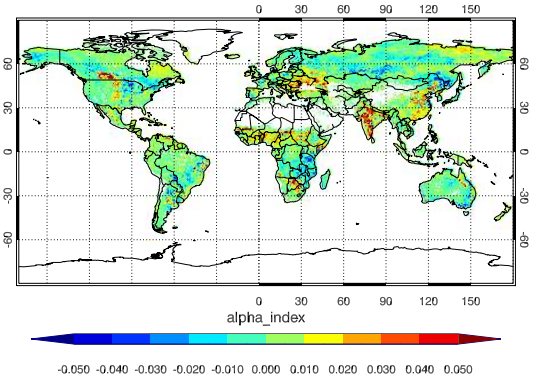

(b) GBAF: Trend in Positive GPP Extremes

Fig. 4: Same as Fig. 3, but for annual block maxima.

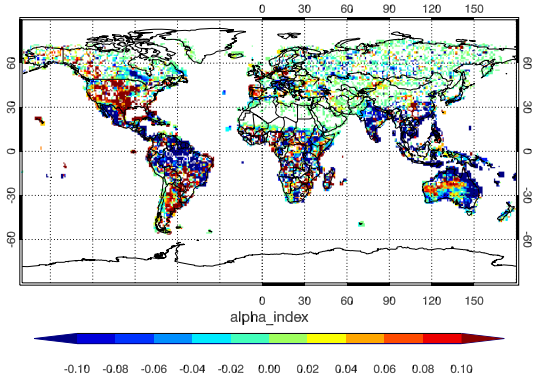

(a) E3SM-BGC: ENSO dependence of Negative GPP Extremes

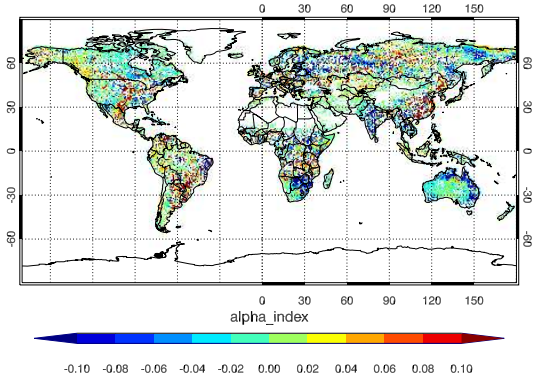

(b) GBAF: ENSO dependence of Negative GPP Extremes

Fig. 5: Geographic distribution of the ENSO-dependent component (α_{ENSO}) of the location parameter of the ENSOGEV model of annual block minima (units: $gCm^{-2}day^{-1}yr^{-1}$ per unit standard deviation of Niño3.4 index) of (a) the E3SM-BGC (1980-2006) and (b) the GBAF data during 1982-2008. Hatching represents regions where ENSOGEV is statistically different than BaseGEV at the 95% confidence level (based on the log-likelihood test and using the false discovery rate approach for establishing statistical significance. Please see main text's Section IIc.)

of the GBAF data are smaller. There are slightly positive trends in northeastern and eastern Amazon, southern Asia, and northern Australia.

There are only a few ENSO events from the 1980s to the 2000s. This small sample size may not be enough to establish robust statistics of the impact of ENSO on carbon extremes. When an ENSOGEV model was fit to annual block maxima/minima for the longer period of 1900-2006 of the E3SM-BGC simulation, statistically significant (at the 95% confidence level) ENSO dependence was noted over parts of Amazon region, maritime continent and Northern Australia with similar magnitudes (not shown here). But, given the limited time period of observational GPP data, that result will be difficult to validate. In the future, we would extend this analysis to other related coupled BGC experiments and CMIP6 results to identify and attribute the plausible pathways of the noted ENSO dependence as well as impact of other modes of variability on carbon extremes.

Many studies have shown that ENSO generally causes climate extremes and eventually will affect carbon cycle and lead to carbon extreme events [36], [37]. To our knowledge, this is first study of linking the carbon extremes and ENSO indices under the GEV statistical model to study the ENSO impacts on carbon extremes.

IV. Conclusions

To evaluate the simulation of carbon extremes by the E3SMv1.1-BGC model, we estimate the GEV statistical models (BaseGEV, timeGEV and ENSOGEV) of extremes in the simulated monthly GPP for the period of 1980-2006 and monthly observational GPP dataset (GBAF) ranging from 1982-2008. We evaluate the stationary component of GPP extremes as well as their trends and the impact of a large scale mode of climate variability, ENSO, on them. These GEV models are fit to annual maxima/minima of monthly GPP anomalies. Our results show that:

1) The magnitudes of location parameters, and thus GPP extremes, from the E3SM-BGC simulation are larger (a factor of three to four in some regions) than those from

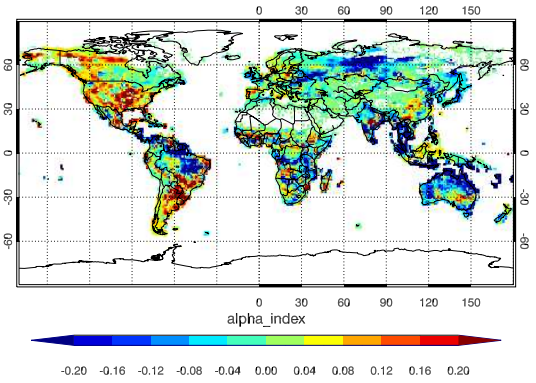

(a) E3SM-BGC: ENSO dependence of Positive GPP Extremes

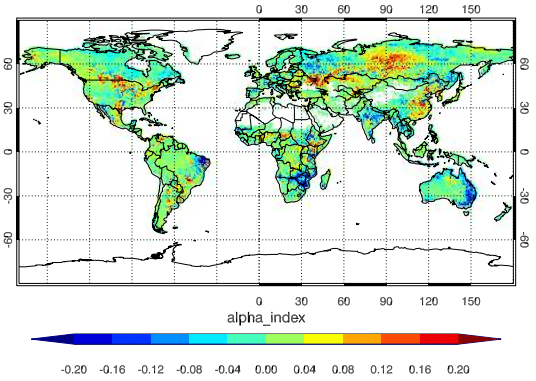

(b) GBAF: ENSO dependence of Positive GPP Extremes

Fig. 6: Same as Fig. 5, except for annual block maxima.

the GBAF data for both positive and negative extremes.

2) the negative GPP extremes are generally more pronounced than the positive extremes both in the E3SM-BGC simulation and GBAF data.
3) The E3SM-BGC simulated positive GPP extremes exhibit significant increasing trends in some regions (Amazon, western Africa, Eurasia, southeastern China, south eastern Australia and the maritime continent). These trends are stronger than observed and no regions exhibit a statistically significant trend in the GBAF data.
4) Large positive trends in the simulated negative GPP extremes are also noted over large areas that are stronger than that exhibited by the GBAF data. But, these trends are not significant either in the E3SM-BGC simulation or GBAF data.
5) For the period of 1980-2006, the simulated GPP negative and positive extremes generally show stronger dependence to ENSO than the GBAF data. However, this ENSO dependence is also not significant either in the E3SM-BGC simulation or GBAF data.
6) However, for the simulated period of 1900-2006, where the sample size is larger, the E3SM-BGC simulation exhibits statistically significant ENSO dependence of negative and positive extremes over Amazon, maritime continent and northern Australia.

ACKNOWLEDGMENT

We thank DOE E3SM CBGC simulation group for coordinating experiments and conducting simulations. This research was supported through the Reducing Uncertainties in Biogeochemical Interactions through Synthesis and Computation Scientific Focus Area (RUBISCO SFA), which are sponsored by the Climate and Environmental Sciences Division (CESD) of the Biological and Environmental Research (BER) Program in the U.S. Department of Energy Office of Science. This research used resources of the National Energy Research Scientific Computing Center, a DOE Office of Science User Facility and the Oak Ridge Leadership Computing Facility at the Oak Ridge National Laboratory, which are supported by the Office of Science of the U.S. Department of Energy under Contract No. DE-AC02-05CH11231 and DE-AC05-00OR22725 respectively.

REFERENCES

[1] F. M. Hoffman, J. T. Randerson, V. K. Arora, Q. Bao, P. Cadule, D. Ji, C. D. Jones, M. Kawamiya, S. Khatiwala, K. Lindsay, A. Obata, E. Shevliakova, K. D. Six, J. F. Tjiputra, E. M. Volodin, and T. Wu, "Causes and implications of persistent atmospheric carbon dioxide biases in Earth System Models," *Journal of Geophysical Research: Biogeosciences*, vol. 119, no. 2, pp. 141–162, Feb. 2014. [Online]. Available: http://doi.wiley.com/10.1002/2013JG002381

[2] S. Bony, G. Bellon, D. Klocke, S. Sherwood, S. Fermepin, and S. Denvil, "Robust direct effect of carbon dioxide on tropical circulation and regional precipitation," *Nature Geoscience*, vol. 6, p. 447, Apr. 2013. [Online]. Available: https://doi.org/10.1038/ngeo1799

[3] J. Zscheischler, M. Reichstein, J. vonButtlar, M. Mu, J. T. Randerson, and M. D. Mahecha, "Carbon cycle extremes during the 21st century in cmip5 models: Future evolution and attribution to climatic drivers," *Geophysical Research Letters*, vol. 41, no. 24, pp. 8853–8861, 2014. [Online]. Available: https://agupubs.onlinelibrary.wiley.com/doi/abs/10.1002/2014GL062409

[4] S. Piao, X. Zhang, A. Chen, Q. Liu, X. Lian, X. Wang, S. Peng, and X. Wu, "The impacts of climate extremes on the terrestrial carbon cycle: A review," *Science China Earth Sciences*, May 2019. [Online]. Available: https://doi.org/10.1007/s11430-018-9363-5

[5] H. S. Baker, R. J. Millar, D. J. Karoly, U. Beyerle, B. P. Guillod, D. Mitchell, H. Shiogama, S. Sparrow, T. Woollings, and M. R. Allen, "Higher CO2 concentrations increase extreme event risk in a 1.5 C world," *Nature Climate Change*, vol. 8, no. 7, pp. 604–608, Jul. 2018. [Online]. Available: http://www.nature.com/articles/s41558-018-0190-1

[6] C. Le Quéré, M. Raupach, J. G. Canadell, G. Marland, L. Bopp, P. Ciais, T. Conway, S. Doney, R. Feely, P. Foster, P. Friedlingstein, K. Gurney, R. Houghton, J. House, C. Huntingford, P. Levy, M. Lomas, J. Majkut, N. Metzl, and I. Woodward, "Trends in the sources and sinks of carbon dioxide," *Nature Geoscience*, vol. 2, pp. 831–836, 11 2009.

[7] P. Ciais, C. Sabine, G. Bala, L. Bopp, V. Brovkin, J. Canadell, A. Chhabra, R. DeFires, J. Galloway, M. Heimann, C. Jones, C. L. Quéré, R. B. Myneni, S. Piao, and P. Thornton, "Carbon and other biogeochemical cycles," Cambridge, United Kingdom and New York, NY, USA, 2013.

[8] P. Friedlingstein, M. Meinshausen, V. K. Arora, C. D. Jones, A. Anav, S. K. Liddicoat, and R. Knutti, "Uncertainties in CMIP5 Climate Projections due to Carbon Cycle Feedbacks," *Journal of Climate*, vol. 27, no. 2, pp. 511–526, Jan. 2014. [Online]. Available: http://journals.ametsoc.org/doi/abs/10.1175/JCLI-D-12-00579.1

[9] M. Reichstein, M. Bahn, P. Ciais, D. Frank, M. D. Mahecha, S. I. Seneviratne, J. Zscheischler, C. Beer, N. Buchmann, D. C. Frank, D. Papale, A. Rammig, P. Smith, K. Thonicke, M. van der Velde, S. Vicca, A. Walz, and M. Wattenbach, "Climate extremes and the carbon cycle," *Nature*, vol. 500, no. 7462, pp. 287–295, Aug. 2013. [Online]. Available: https://www.nature.com/articles/nature12350

[10] S. L. Lewis, P. M. Brando, O. L. Phillips, G. M. F. v. d. Heijden, and D. Nepstad, "The 2010 Amazon Drought," *Science*, vol. 331, no. 6017, pp. 554–554, Feb. 2011. [Online]. Available: http://science.sciencemag.org/content/331/6017/554

[11] C. Potter, S. Klooster, C. Hiatt, V. Genovese, and J. C. Castilla-Rubio, "Changes in the carbon cycle of amazon ecosystems during the 2010 drought," *Environmental Research Letters*, vol. 6, no. 3, p. 034024, jul 2011. [Online]. Available: https://doi.org/10.1088/1748-9326/6/3/F034024

[12] V. V. Kharin and F. W. Zwiers, "Estimating extremes in transient climate change simulations," *Journal of Climate*, vol. 18, no. 8, pp. 1156–1173, 2005. [Online]. Available: https://doi.org/10.1175/JCLI3320.1

[13] S. J. Brown, J. Caesar, and C. A. T. Ferro, "Global changes in extreme daily temperature since 1950," *J. Geophys. Res.*, vol. 113, no. D5, 03 2008. [Online]. Available: http://dx.doi.org/10.1029/2006JD008091

[14] K. J. Evans, S. Mahajan, M. Branstetter, J. L. McClean, J. Caron, M. E. Maltrud, J. J. Hack, D. C. Bader, R. Neale, and J. K. Leifeld, "A spectral transform dynamical core option within the Community Atmosphere Model (CAM4)," *Journal of Advances in Modeling Earth Systems*, vol. 6, no. 3, pp. 902–922, 2014. [Online]. Available: http://dx.doi.org/10.1002/2014MS000329

[15] M. F. Wehner, K. A. Reed, F. Li, Prabhat, J. Bacmeister, C.-T. Chen, C. Paciorek, P. J. Gleckler, K. R. Sperber, W. D. Collins, A. Gettelman, and C. Jablonowski, "The effect of horizontal resolution on simulation quality in the Community Atmospheric Model, CAM5.1," *Journal of Advances in Modeling Earth Systems*, vol. 6, no. 4, pp. 980–997, 2014. [Online]. Available: http://dx.doi.org/10.1002/2013MS000276

[16] S. Mahajan, K. J. Evans, M. Branstetter, V. Anantharaj, and J. K. Leifeld, "International conference on computational science, iccs 2015 fidelity of precipitation extremes in high resolution global climate simulations," *Procedia Computer Science*, vol. 51, pp. 2178 – 2187, 2015. [Online]. Available: http://www.sciencedirect.com/science/article/pii/S1877050915013009

[17] S. Mahajan, K. J. Evans, M. L. Branstetter, and Q. Tang, "Model resolution sensitivity of the simulation of north atlantic oscillation teleconnections to precipitation extremes," *Journal of Geophysical Research: Atmospheres*, vol. 123, no. 20, pp. 11,392–11,409, 2018. [Online]. Available: https://agupubs.onlinelibrary.wiley.com/doi/abs/10.1029/2018JD028594

[18] K. Whan and F. Zwiers, "The impact of enso and the nao on extreme winter precipitation in north america in observations and regional climate models," *Climate Dynamics*, vol. 48, no. 5, pp. 1401–1411, Mar 2017. [Online]. Available: https://doi.org/10.1007/s00382-016-3148-x

[19] S. D. Sippel, "Climate extremes and their impact on ecosystem-atmosphere interactions," Ph.D. dissertation, ETH Zurich, 2017.

[20] S. Sippel, D. Mitchell, M. T. Black, A. J. Dittus, L. Harrington, N. Schaller, and F. E. L. Otto, "Combining large model ensembles with extreme value statistics to improve attribution statements of rare events," *Weather and Climate Extremes*, vol. 9, pp. 25 – 35, 2015. [Online]. Available: http://www.sciencedirect.com/science/article/pii/S2212094715300050

[21] F. Tonini, G. J. Lasinio, and H. H. Hochmair, "Mapping return levels of absolute NDVI variations for the assessment of drought risk in Ethiopia," *International Journal of Applied Earth Observation and Geoinformation*, vol. 18, pp. 564 – 572, 2012. [Online]. Available: http://www.sciencedirect.com/science/article/pii/S0303243412000621

[22] J. J. Martn-Sotoca, A. Saa-Requejo, R. Moratiel, N. Dalezios, I. Faraslis, and A. M. Tarquis, "Statistical analysis for satellite-index-based insurance to define damaged pasture thresholds," *Natural Hazards and Earth System Sciences*, vol. 19, no. 8, pp. 1685–1702, Aug. 2019. [Online]. Available: https://www.nat-hazards-earth-syst-sci.net/19/1685/2019/

[23] J. Zscheischler, M. D. Mahecha, J. von Buttlar, S. Harmeling, M. Jung, A. Rammig, J. T. Randerson, B. Schlkopf, S. I. Seneviratne, E. Tomelleri, S. Zaehle, and M. Reichstein, "A few extreme events dominate global interannual variability in gross primary production," *Environmental Research Letters*, vol. 9, no. 3, p. 035001, mar 2014. [Online]. Available: https://doi.org/10.10881748-932693035001

[24] Chen, "Negative extreme events in gross primary productivity and their drivers in china during the past three decades," *Agricultural and Forest Meteorology*, 2019.

[25] V. Eyring, S. Bony, G. A. Meehl, C. A. Senior, B. Stevens, R. J. Stouffer, and K. E. Taylor, "Overview of the coupled model intercomparison project phase 6 (cmip6) experimental design and organization," *Geoscientific Model Development*, vol. 9, no. 5, pp. 1937–1958, 2016. [Online]. Available: https://www.geosci-model-dev.net/9/1937/2016/

[26] J.-C. Golaz, P. M. Caldwell, L. P. Van Roekel, M. R. Petersen, Q. Tang, J. D. Wolfe, G. Abeshu, V. Anantharaj, X. S. Asay-Davis, D. C. Bader, S. A. Baldwin, G. Bisht, P. A. Bogenschutz, M. Branstetter, M. A. Brunke, S. R. Brus, S. M. Burrows, P. J. Cameron-Smith, A. S. Donahue, M. Deakin, R. C. Easter, K. J. Evans, Y. Feng, M. Flanner, J. G. Foucar, J. G. Fyke, B. M. Griffin, C. Hannay, B. E. Harrop, E. C. Hunke, R. L. Jacob, D. W. Jacobsen, N. Jeffery, P. W. Jones, N. D. Keen, S. A. Klein, V. E. Larson, L. R. Leung, H.-Y. Li, W. Lin, W. H. Lipscomb, P.-L. Ma, S. Mahajan, M. E. Maltrud, A. Mametjanov, J. L. McClean, R. B. McCoy, R. B. Neale, S. F. Price, Y. Qian, P. J. Rasch, J. J. Reeves Eyre, W. J. Riley, T. D. Ringler, A. F. Roberts, E. L. Roesler, A. G. Salinger, Z. Shaheen, X. Shi, B. Singh, J. Tang, M. A. Taylor, P. E. Thornton, A. K. Turner, M. Veneziani, H. Wan, H. Wang, S. Wang, D. N. Williams, P. J. Wolfram, P. H. Worley, S. Xie, Y. Yang, J.-H. Yoon, M. D. Zelinka, C. S. Zender, X. Zeng, C. Zhang, K. Zhang, Y. Zhang, X. Zheng, T. Zhou, and Q. Zhu, "The doe e3sm coupled model version 1: Overview and evaluation at standard resolution," *Journal of Advances in Modeling Earth Systems*, vol. 11, no. ja, 2019. [Online]. Available: https://agupubs.onlinelibrary.wiley.com/doi/abs/10.1029/2018MS001603

[27] S. M. Burrows, M. Maltrud, X. Yang, Q. Zhu, N. Jeffery, X. Shi, D. Ricciuto, S. Wang, G. Bisht, J. Tang, J. Wolfe, B. E. Harrop, B. Singh, L. Brent, T. Zhou, P. Cameron-Smith, N. Keen, N. Collier, M. Xu, S. M. E. E. C. Hunke, A. K. Turner, H. Li, H. Wang, J.-C. Golaz, B. Bond-Lamberty, F. M. Hoffman, W. J. Riley, P. E. Thornton, K. Calvin, and L. R. Leung, "The doe e3sm coupled model v1.1 biogeochemistry configuration: overview and evaluation of coupled carbon-climate experiments," *Journal of Advances in Modeling Earth Systems*, under review.

[28] J. K. Moore, S. C. Doney, J. A. Kleypas, D. M. Glover, and I. Y. Fung, "An intermediate complexity marine ecosystem model for the global domain," *Deep Sea Research Part II: Topical Studies in Oceanography*, vol. 49, no. 1-3, pp. 403–462, 2001.

[29] J. K. Moore, S. C. Doney, and K. Lindsay, "Upper ocean ecosystem dynamics and iron cycling in a global three-dimensional model," *Global Biogeochemical Cycles*, vol. 18, no. 4, 2004.

[30] M. Jung, M. Reichstein, H. A. Margolis, A. Cescatti, A. D. Richardson, M. A. Arain, A. Arneth, C. Bernhofer, D. Bonal, J. Chen, D. Gianelle, N. Gobron, G. Kiely, W. Kutsch, G. Lasslop, B. E. Law, A. Lindroth, L. Merbold, L. Montagnani, E. J. Moors, D. Papale, M. Sottocornola, F. Vaccari, and C. Williams, "Global patterns of land-atmosphere fluxes of carbon dioxide, latent heat, and sensible heat derived from eddy covariance, satellite, and meteorological observations," *J. Geophys. Res.*, vol. 116, p. G00J07, 2011. [Online]. Available: http://dx.doi.org/10.1029/2010JG001566

[31] M. Xu, X.-Z. Liang, A. Samel, and W. Gao, "MODIS Consistent Vegetation Parameter Specifications and Their Impacts on Regional Climate Simulations," *Journal of Climate*, vol. 27, no. 22, pp. 8578–8596, Aug. 2014. [Online]. Available: http://journals.ametsoc.org/doi/abs/10.1175/JCLI-D-14-00082.1

[32] J. E. Heffernan and A. G. Stephenson, *ismev: An Introduction to Statistical Modeling of Extreme Values*, 2018, R package version 1.42. [Online]. Available: https://CRAN.R-project.org/package=ismev

[33] S. G. Coles, *An Introduction to Statistical Modeling of Extreme Values*. Springer, 2001.

[34] D. S. Wilks, "On field significance and the false discovery rate," *Journal of Applied Meteorology and Climatology*, vol. 45, no. 9, pp. 1181–1189, 2006. [Online]. Available: https://doi.org/10.1175/JAM2404.1

[35] V. Ventura, C. J. Paciorek, and J. S. Risbey, "Controlling the proportion of falsely rejected hypotheses when conducting multiple tests with climatological data," *Journal of Climate*, vol. 17, no. 22, pp. 4343–4356, 2004. [Online]. Available: https://doi.org/10.1175/3199.1

[36] C. D. Jones, M. Collins, P. M. Cox, and S. A. Spall, "The carbon cycle response to enso: A coupled climatecarbon cycle model study," *Journal of Climate*, vol. 14, no. 21, pp. 4113–4129, 2001. [Online]. Available: https://doi.org/10.1175/1520-0442(2001)014¡4113:TCCRTE¿2.0.CO;2

[37] W. Cai, A. Santoso, G. Wang, S.-W. Yeh, S.-I. An, K. M. Cobb, M. Collins, E. Guilyardi, F.-F. Jin, J.-S. Kug, M. Lengaigne, M. J. McPhaden, K. Takahashi, A. Timmermann, G. Vecchi, M. Watanabe, and L. Wu, "ENSO and greenhouse warming," *Nature Climate Change*, vol. 5, no. 9, pp. 849–859, Sep. 2015. [Online]. Available: https://www.nature.com/articles/nclimate2743